Journal of Chromatography, 149 (1978) 465–487

CHROM. 10,840

BROAD-RANGE LINEAR CALIBRATION IN HIGH-PERFORMANCE SIZE-EXCLUSION CHROMATOGRAPHY USING COLUMN PACKINGS WITH BIMODAL PORES

W. W. YAU, C. R. GINNARD and J. J. KIRKLAND

E. I. du Pont de Nemours and Company, Central Research & Development Department, Experimental Station, Wilmington, Del. 19898 (U.S.A.)

SUMMARY

The linear size-separation range for size-exclusion chromatography (SEC) (gel permeation chromatography) is greatly extended by optimizing the pore-size distribution and the internal pore volume of particles in the columns. This approach permits easier, more accurate computation of molecular weights by the "single broad standard" method, which assumes a linear calibration graph. Linearities of 4–5 decades of molecular weight have been demonstrated, in comparison to the 2.5–3 decades of linearity obtained with conventional column arrangements. The new concept is to couple SEC columns containing only two discrete pore sizes, (bimodal), having about one decade difference in pore size and approximately equal pore volumes for the two pore sizes. This is in sharp contrast to the widely accepted approach of connecting several columns containing several packing materials of slightly different pore sizes and pore volumes. The desired pore sizes of this bimodal distribution are arranged so that the linear portion of the individual column molecular weight calibration graphs is substantially non-overlapping, and the pore volume of each mode is such that the linear portions of the calibration graphs are essentially parallel. The theoretical support and quantitative optimization guidelines for the bimodal approach of practical column selection are provided.

The wide-linear molecular weight calibration also has been demonstrated with columns of new 10-μm single bimodal pore-size silica particles with narrow pore-size distributions. The use of a single packing material for SEC greatly simplifies column inventory and improves convenience, while maintaining the high chromatographic resolution and accurate molecular weight measurements associated with high-performance SEC.

INTRODUCTION

Historically, pore sizes (PS) of column sets for size-exclusion chromatography (SEC) (or gel permeation chromatography, GPC) have been selected by empirical guidelines. One popular guideline recommends a column of each pore size that

has fractionation capability in the molecular weight (MW) range of the polymer[1,2]. In effect, this broadens the pore-size distribution (PSD) of packing within the combined column set. We find that this approach is not as effective as a bimodal PSD in widening the useful linear MW separation range. The present study shows the importance of uniformly distributing the resolution of a column set over a wide MW range to achieve maximum GPC MW accuracy.

SEC (or GPC) has a finite overall separation capacity. The range of peak retention volumes (total exclusion, total permeation) is limited by the total pore volume of the column packing. For GPC columns of a single PS, this separation capacity is concentrated in a narrow MW range. Thus, the resolution of columns with a single PS is high, but the relatively narrow MW range limits their use only to GPC analyses of narrow MW distribution (MWD) polymers.

In practice, GPC columns of different PS are commonly connected to provide a wider MW separation range. If this wider MW separation range is accomplished by using an effective broad PSD, the resolution of the combined column set is less than that of single columns of a single PS (of the same length). However, this sacrifice in resolution is modest compared with the gain in increased convenience and versatility of a wide MW range column set. This is especially true for high-performance GPC columns ($<10\,\mu$m particles). In this instance some sacrifice in resolution creates only a minor effect on MW errors[3]. Most GPC laboratories prefer convenient systems that provide a wide MW separation range to analyse polymers of different MW and MWD without having to change and re-calibrate column sets.

In the approach proposed here, columns with packings of only two PS (*i.e.*, bimodal PSD) are used. With proper selection of these two PS, a bimodal column set can give a wider useful MW separation range and a more even distribution of MW resolution than conventional methods. Therefore, greater flexibility, convenience and accuracy of MW measurements result.

In this paper, we describe a quantitative theory of the bimodal PSD concept for selecting GPC columns. The study was accomplished by computer simulation using accepted relationships for: (1) the shape of the GPC calibration graph for a single PS, (2) the polymer MWD and (3) the packing PSD curves. Results of the simulation describe how the MW range and accuracy of GPC MW determinations are effected by the PS combinations of different column sets. The simplicity and the improved MW accuracy of a bimodal PS column set are demonstrated by the simulation. Also given are practical guidelines for arranging commercially available columns in a bimodal configuration.

The results of the present simulation study allow the prediction of the PS, PSD and relative pore volumes of the bimodal systems to compromise between or attain either goal: wide MW calibration range for convenience and versatility, or a close linear fit of the calibration graph for maximal accuracy of MW determination. Optimized configurations are compared to results with particles of mono-modal pores with various size distributions. The performance of column sets with various PS differences and distributions is judged according to expected MW accuracy for a typical polymer sample by simulated GPC analyses.

The wide-linear MW calibration also has been demonstrated with columns of a new 10-μm single bimodal PS silica particle with narrow PSD. The use of a single packing material for GPC greatly simplifies column inventory and improves conve-

nience, while maintaining the high chromatographic resolution and accurate MW measurements associated with high-performance GPC.

MATERIALS AND METHODS

Apparatus

Column data on the porous silica microsphere (PSM) particles were obtained at ambient temperature on an apparatus consisting of an Altex Model 100-A solvent metering system (Altex Scientific, Berkeley, Calif., U.S.A.), and a DuPont Model 410 UV photometric detector (Instrument Products Div., DuPont, Wilmington, Del., U.S.A.) with a 1-μl ultramicroabsorption cell[4]. Samples were introduced into columns with an external sample loop using a Model CV-6UHPa-C-20 microsampling valve (Valco Instrument Co., Houston, Texas, U.S.A.). Columns were made from precision-bore, stainless-steel tubing manufactured by the Superior Tubing Co. (Norristown, Pa., U.S.A.). This tubing is described as Type 316L super-pressure tubing with an inside mirror finish. Stainless-steel compression fittings (Swagelok Fitting Co., Cleveland, Ohio, U.S.A.) were modified for minimal dead-volume and unobstructed flow-through patterns[4]. Column blanks were carefully cleaned before use[5], and packed columns were connected when required with 2-cm lengths of 0.025-cm I.D. capillary tubing using appropriate low-dead-volume fittings.

Reagents and chromatographic particles

Tetrahydrofuran was distilled-in-glass material from Burdick & Jackson Labs. (Muskegon, Mich., U.S.A.). PSM packings were prepared by the techniques previously described[6–8]. Inquiries on columns of similar particles utilizing the bimodal PSD technology should be directed to the Instrument Products Division, E. I. du Pont de Nemours & Co., Wilmington, Del. 19898, U.S.A. (patents pending). Synthesis of bimodal silica particles is described in the text. Polystyrene standards were obtained from Pressure Chemical Co., Pittsburgh, Pa., U.S.A.

μ-Styragel columns were procured from Waters Assoc. (Milford, Mass., U.S.A.). Data on these columns were obtained at ambient temperature using a Model 1010B liquid chromatograph (Hewlett-Packard, Avondale, Pa., U.S.A.) with a Model 770 differential refractometer detector (Micromeritics, Norcross, Ga., U.S.A.).

Column packing techniques

Columns were prepared by the high-pressure filtration (slurry) method using the equipment and technique described previously[9]. A methanol–chloroform (1:1) mixture was used as a suspending liquid for the PSM particles. Packed beds were consolidated at 10,000 p.s.i. to ensure mechanical stability[9].

Data handling and calculations

Column performance data were obtained with a supplementary program on the DuPont Experimental Station PDP-10 real-time computer system[10,11]. Column plate heights were derived from peak areas using the method of James and Martin[12].

CONCEPTS

Fractionation of a range of molecular weights is possible with pores of only one size

This is an often-neglected concept, possibly because it goes against intuitive expectations. It is often mistakenly assumed that a broad spectrum of PS is required for the pore structure to effectively fractionate broad MWD polymers. This misconception has formed the basic philosophy of the conventional and empirical practice of GPC column selection. We find that it is not necessary to have several PS in the resolving column set.

It is not widely appreciated that a single PS is capable of fractionating over a substantial MW range (1.5–2 decades). Fig. 1 illustrates how a single pore separates solute molecules of different sizes by a simple solute-to-wall exclusion effect inside the pore. Because of steric interference, the center of the incoming solute molecules is forced away from the inside walls of the pore, as illustrated by the inner broken line. Smaller molecules can approach closer to the wall, as represented by the outer broken line. Thus, a larger fraction of the pore volume is accessible to smaller molecules than it is to larger molecules. This causes the small molecules to elute later and be separated from large molecules.

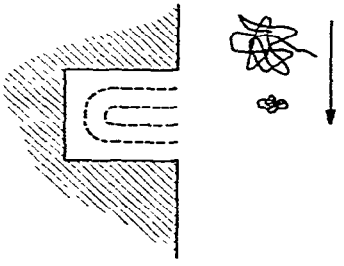

Fig. 1. Size-exclusion effect in a single pore.

For random coil solute molecules as illustrated in Fig. 1, the broken lines are merely oversimplified representations of the extent of the wall exclusion. Actually, the wall exclusion effect is due to the progressively increased restriction of the conformational freedom (decreased entropy) of the solute molecules near the wall. For solid-sphere molecules, the broken lines can actually represent the well defined wall-exclusion boundary. In this instance, wall exclusion is related to the fact that the center of the sphere has to be a distance of one radius from the wall.

The exclusion effect illustrated in Fig. 1 is an acceptable explanation for GPC separation. Casassa and Tagami[13] developed a quantitative GPC theory of this effect for random coil type solute molecules for a cylindrical pore shape model of single pore size:

$$K_{GPC} = 4 \sum_{m=1}^{\infty} \beta_m^{-2} \exp\left(-\beta_m^2 R_g^2/a^2\right) \tag{1}$$

where K_{GPC} = GPC distribution coefficient[14], which is assumed to be equivalent to the accessible pore volume fraction, R_g = radius of gyration of the solute, a = pore radius and β_m = numerical constant equal to the mth root for the Bessel function of the first kind of order zero. Eqn. 1 predicts how GPC peak retention measured by K_{GPC} varies with R_g of the random coil polymer molecules, and it is the equation which relates the GPC calibration graph to moleculer size.

To convert molecular size, R_g, into molecular weight, MW (or M):

$$R_g = k\,M^{\alpha} \tag{2}$$

where k and α are constants having specific values for different polymer–solvent systems (the usual value of α is between 0.5 and 0.6). Values for k and α can be easily calculated if the Mark–Houwink constants of the viscosity–MW relationship are known[15]. With published Mark–Houwink constants[16], we find that the specific R_g and MW conversion for polystyrene in tetrahydrofuran (THF) takes the form

$$R_g = 0.137\,M^{0.589}\ \text{Å} \tag{3}$$

Use of eqn. 3 in conjunction with eqn. 1 allows construction of the theoretical GPC calibration graph for polystyrene in THF, assuming cylindrical pores of single PS (this is the curve shown at the top right-hand side of Fig. 3 with the ordinate in the log MW scale. The scale for a 1-decade MW separation is indicated below the calibration graphs. Comparing the top curve with this MW scale, it can be seen that a single PS can cover about 1½ decades of MW separation range).

Linear calibration approximation is needed to simplify GPC molecular weight computation

Exact GPC calibration is experimentally possible if several narrow MWD standards of different known MWs are available for the polymer of interest. One simply obtains the GPC curves for the standards and plots the logarithm of the known MW *versus* the GPC peak retention parameter (*e.g.*, K_{GPC}). Unfortunately, for polymers other than polystyrene, narrow standards are not generally available for this procedure. One useful solution to this problem is to use a single broad MWD polymer standard for calibrating the GPC columns[17]. Broad standards of known weight- and number-average MW ($\bar{M}_w$, $\bar{M}_n$) are available for many commercial polymers. Unknown polymer samples also can be converted to standards by measuring its $\bar{M}_w$ and $\bar{M}_n$ using recognized light-scattering and osmometric techniques. However, the price one must pay for the practical convenience of the broad MWD single standard calibration approach is that resultant calibration gives only a linear approximation of the exact calibration graph. This approach then places a linear calibration requirement for the columns in a selected set. Therefore, to obtain meaningful and useful calibration, a wide linear calibration range is required.

As the MW separation capacity is directly related to the slope of the calibration graph, the linearity of the calibration graph of a column set is a measure of how evenly the column resolution is distributed over the MW range. The linearity is, in turn, measured by how well the calibration graph can be fitted to a straight line.

SIMULATION STUDY OF GPC CALIBRATION GRAPH SHAPES

Definitions, assumptions and conventions

Casassa and Tagami's GPC theory[13] of the random coil molecule and the cylindrical pore shape (eqn. 1) is the primary model used for the computer-simulation study. A slab pore shape was considered in one instance for comparison.

The theoretical GPC calibration graphs for pores having finite PSD are calculated by averaging the individual calibration graphs for each pore, weighted by its volume fraction, over the entire PSD range. The shape of the PSD curve assumes the form of the log-normal distribution. The choice of this curve shape over the linear gaussian PSD curve shape is suggested by the fact that experimental PSD curves (*e.g.*, mercury intrusion) are always presented in the log PS scale. When plotted on the log-scale, the log-normal distribution curve takes on the gaussian curve shape. Fig. 2 shows two of these curves with PSD values of 0.15 and 0.65. The values of PSD are the standard deviation of the curves in units of Δlog PS. At PSD = 0.15, the ratio of the PS at one standard deviation is $10^{0.15}$, or 1.4. For this distribution, the base of the PSD curve covers 1 decade in PS. On the other hand, at PSD = 0.65, the PS ratio for one standard deviation becomes $10^{0.65}$, or 4.5, and the base extends more than 2 decades in PS. Experimental PSD curves of this latter broad distribution are not commonly observed among rigid GPC packings.

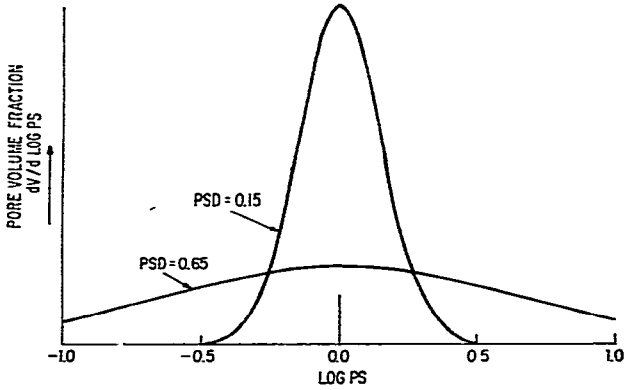

Fig. 2. Log-normal pore size distribution shape.

The convention used in displaying the data from the simulation study is illustrated in Fig. 3. The plot on the right shows how the GPC calibration graph changes from single pore size (*i.e.*, PSD = 0) to monomodal pores with PSD = 0.15 and 0.65. The three corresponding PSD curve shapes are inserted to the left of these calibration graphs in the figure for convenient identification. The dashed lines in Fig. 3 are the linear approximation of the three calibration graphs obtained by the least-squares fit to the solid calibration graphs between $K_{GPC} = 0$ and 0.9.

On the left of Fig. 3 is shown the separation range, I_R, reported in decades of R_g, calculated as the difference in log R_g at the limits, that is:

$$I_R = (\Delta \log R_g)_{K_{GPC}\,:\,0 \text{ to } 0.9} \tag{4}$$

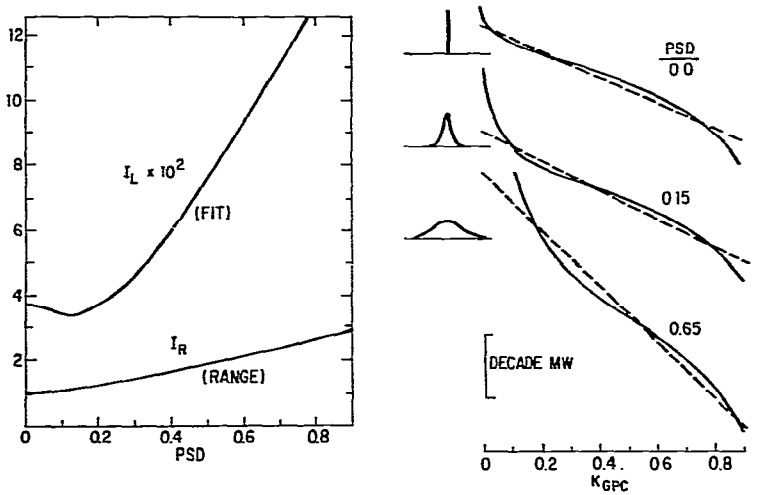

Fig. 3. Effect of pore size distribution on calibration linearity and molecular weight range for size-exclusion chromatography: monomodal.

The conversion of I_R into polystyrene MW separation range, I_{MW}, can be accomplished by

$$I_{MW} = I_R/0.589 \tag{5}$$

Eqn. 5 is given in Table I for easier reference. The "goodness" of the linear fit (*e.g.*, dashed line in Fig. 3) is determined by the inherent linearity of the theoretical calibration graphs. This fit is measured by the index of linearity, I_L, which is calculated as the root-mean-square deviation of the fit in the log R_g units:

$$I_L = [\Sigma(\Delta \log R_g)^2/n]^{\frac{1}{2}} \tag{6}$$

where $\Delta \log R_g$ is the difference in log R_g between the theoretical and the linear calibration graphs at the same K_{GPC} values. The number of data points used to calculate I_L

TABLE I

CONVERSION BETWEEN GPC SEPARATION RANGES

I_R in decades of R_g (radius of gyration)	*I_{MW} in decades of molecular weight (polystyrene)*
1.0	1.70
1.2	2.04
1.4	2.38
1.6	2.72
1.8	3.06
2.0	3.40
2.2	3.74
2.4	4.07
2.6	4.41
2.8	4.75
3.0	5.09

is represented by n in eqn. 6. Thus, I_L is the standard deviation of the linear fit of the GPC calibration graph.

The average errors in determining R_g are related to I_L by:

$$R_g \text{ error } (\%) = (10^{I_L} - 1) \cdot 100 \tag{7}$$

Based on eqn. 3, the average MW errors will then be

$$\varepsilon_{MW} = (10^{I_L} - 1) \cdot 100/0.589 \tag{8}$$

As larger $\Delta \log R_g$ values in eqn. 6 are more heavily weighted than smaller deviations, the ε_{MW} value calculated from eqn. 8 approximately represents the maximum MW error that can be anticipated from a linear approximation of the GPC calibration graph. This error is related to the uncertainty in determining the MW of narrow MWD samples. Eqn. 8 is given in Table II for easier reference.

TABLE II

CONVERSION BETWEEN I_L AND POLYSTYRENE ε_{MW}

I_L (linearity index)	ε_{MW} (% MW error)
0.00	0.0
0.01	4.0
0.02	8.0
0.03	12.1
0.04	16.4
0.05	20.7
0.06	25.2
0.07	29.7
0.08	34.3
0.09	39.1
0.10	44.0
0.11	48.9
0.12	54.0

To evaluate the performance of different column sets for analyzing broad MWD polymers, we chose a model polymer sample with the Flory or most probable MWD[18]. This MWD model is generally applicable to condensation polymers such as polyamides and polyesters. The weight fraction, W_M, of this MWD can be expressed as follows:

$$W_M = (1 - p)^2 \left(\frac{M}{M_0^2}\right) p^{\left(\frac{M}{M_0} - 1\right)} \tag{9}$$

where p = the extent of reaction and M_0 is the MW of the repeating units. For high MW polymers, p approaches unity and the polydispersity ($\bar{M}_w/\bar{M}_n$) of the polymer approaches 2. When the polymer is fractionated in the linear regions of the GPC calibration graph, the MW corresponding to the GPC elution peak is expected to be the $\bar{M}_w$ of the sample. The exact MWD used in the study is shown in Fig. 4, where

the distribution is plotted in the log MW scale. From Fig. 4, it can be seen that the Flory MWD extends 2 decades in MW at the base. To estimate the MW error in the simulation, this Flory MWD sample was allowed to elute at different peak K_{GPC} locations (*i.e.*, over the calibration graph). The percentage $\bar{M}_w$ and $\bar{M}_n$ errors were then calculated from the corresponding MW differences between the linear and theoretical calibration graphs and plotted as a function of peak K_{GPC} (Figs. 5, 7, 9 and 11).

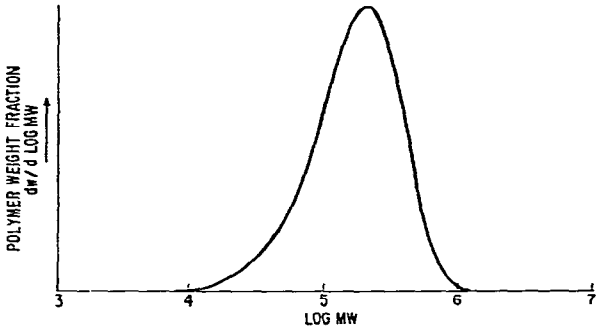

Fig. 4. Most probable (Flory) molecular weight distribution.

Results

The computer-calculated results are grouped into three categories: (1) monomodal pores of broad PSD; (2) bimodal pores with two single PS; and (3) bimodal pores with PSDs.

The results of the study of monomodal pores are shown in Figs. 3 and 5. Fig. 3 shows that the separation range (I_R) increases with increasing PSD. However, the fit (I_L) becomes poorer beyond PSD = 0.15, where I_L reaches a minimum. For PSDs of 0 and 0.15, the MW range of the calibration graph is too narrow to fit a Flory MWD comfortably. Thus, the "wings" of the Flory distribution curve are forced to the extremes of the linear MW range where the linear calibration approximation shows greatest deviation from the theoretical calibration graph. This explains why the MW errors in Fig. 5 for the Flory MWD sample are large for small PSD values. For these monomodal pores, the MW error in $\bar{M}_n$ exceeds 20%, except for samples eluted at peak K_{GPC} in a narrow range around 0.2. The error in $\bar{M}_w$ is lower, partly because the MWD curve is not as skewed at the high MW end. As PSD is increased to 0.65, the linear MW range expands to 4 decades, which serves to reduce the MW errors of broad MWD samples. However, at PSD = 0.65, the fit (I_L) is much poorer, resulting in a higher average MW error, ε_{MW} (up to 45%). This result implies that broadening the monomodal PSD cannot simultaneously produce a wide MW calibration range and a precise fit for low MW errors in both broad and narrow MWD sample analyses. Fig. 5 also shows that peaks eluted at small K_{GPC} values have lower MW errors than those at large K_{GPC}, partly because of the Flory MWD skew at the low MW end.

Figs. 6 and 7 show the effects for bimodal systems with only two single PS. The separation of the two PS again is illustrated by the sketches in the center of Fig. 6 adjacent to the corresponding theoretical calibration graphs. The two sharp lines rep-

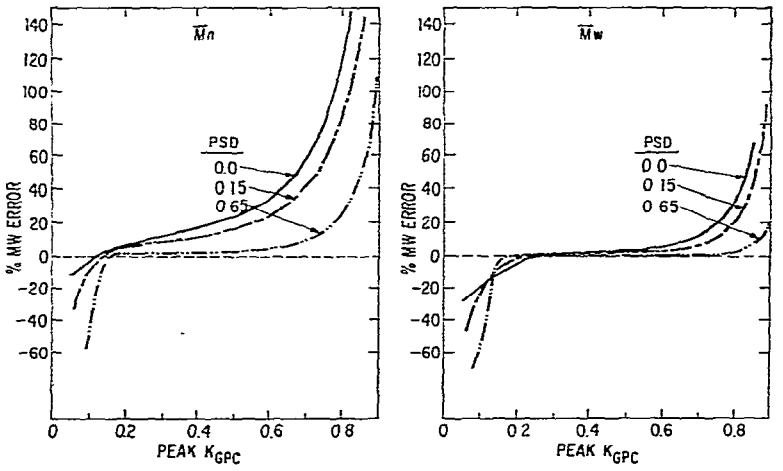

Fig. 5. Effect of polymer with Flory molecular weight distribution on molecular weight errors: monomodal. $\bar{M}_n$ = number-average molecular weight; $\bar{M}_w$ = weight-average molecular weight: K_{GPC} = distribution coefficient corresponding to elution peak.

resenting zero PSD are drawn to equal height to show that the pore volume of the bimodal PS is assumed equal in this instance, $VPR = 1$, where VPR is derived as the pore volume ratio of the large pores to the small pores. VP_2/VP_1 in the bimodal PSD combination. Single or monodispersed pores are, of course, just a theoretical simplification; in practice this roughly corresponds to pores of negligible PSD. The separation of the two PS is measured by Δlog PS values, which are indicated adjacent to the corresponding theoretical and linear calibration graphs. At the left of Fig. 6 the fit (I_L) and the range (I_R) are plotted as a function of PS difference. As the difference in pore size increases, I_R increases steadily. However, I_L goes through a minimum at Δlog

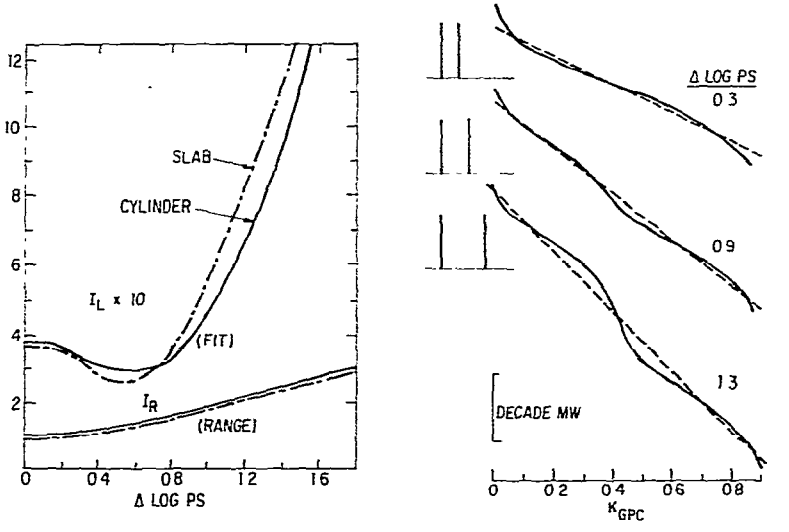

Fig. 6. Effect of pore size distribution on calibration linearity and molecular weight range: bimodal. Pore size distribution (PSD) = 0; pore volume ratio (VPR) = 1.0.

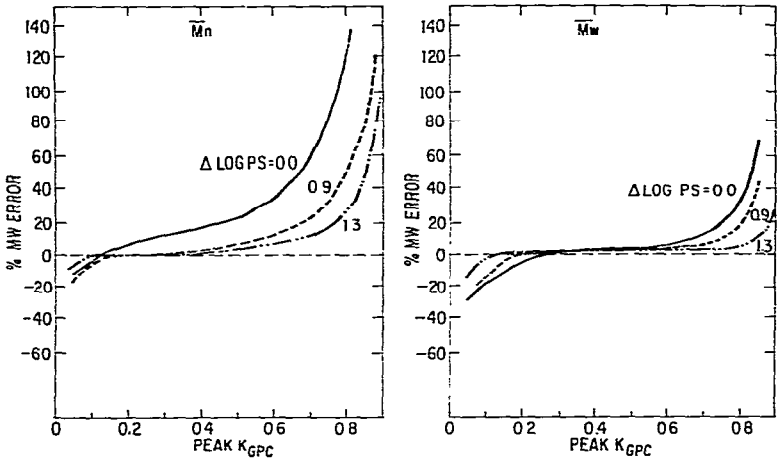

Fig. 7. Effect of polymer with Flory molecular weight distribution on molecular weight errors: bimodal. Conditions as in Fig. 6.

PS $\approx$0.6, then increases sharply. The expected MW error of the broad MWD sample analysis is plotted in Fig. 7 as a function of the peak K_{GPC} of the polymer sample. The plot labeled Δlog PS = 0.0 is for a single PS, which is plotted here for comparison. At Δlog PS = 0.3, the fit is adequate but the MW range is not sufficiently wide to improve significantly on the MW error found for a broad MW sample. However, the PS separation at Δlog PS = 0.9 gives a reasonable compromise in fit and linear range. The bimodal PS condition gives a reasonable linearity fit of $I_L = 0.038$, which corresponds to a ε_{MW} error of 15%. This performance compares very favorably with that of a monomodal PSD situation of comparable MW range, *e.g.*, the monomodal PSD of 0.65 as shown in Figs. 3 and 5, which gives ε_{MW} as high as 45%. As the PS separation becomes too large, the two individual calibration graphs do not meet adequately, creating a resolution gap at the middle of the calibration graph. This results in a poor fit, as illustrated by the line labeled Δlog PS = 1.3 in Fig. 6. The I_L and I_R graphs calculated with an alternative slab pore-shape model[13] are also plotted in Fig. 6 for comparison. The difference in curve shape from the difference in pore shape assumption is small and does not affect the general trend of the data or the conclusions drawn.

The performance of the bimodal PS approach for column selection is further improved by broadening of each of the two groups of pores, as shown in Fig. 8. These data show that a column set of bimodal PSD at Δlog PS = 1.2 will have 4 decades of linear MW range with excellent linear fit. This arrangement also allows good MW accuracy in analysing broad MWD samples, as illustrated in Fig. 9. The curves at Δlog PS of 0.9 are also shown in Fig. 9 for comparison. These plots illustrate that there is some leeway in selecting the PS separation of the bimodal system around the optimum, because of the slow change in I_R and the broadness of the I_L minimum (Fig. 8).

The effect of pore volume ratios in the bimodal PS selection process is illustrated in Fig. 10. Here two PS peaks are sketched with different heights to represent the pore volume ratio. The pore volume ratios also are indicated on the individual calibration graphs, which were calculated using PSD = 0.15 and Δlog PS = 0.9.

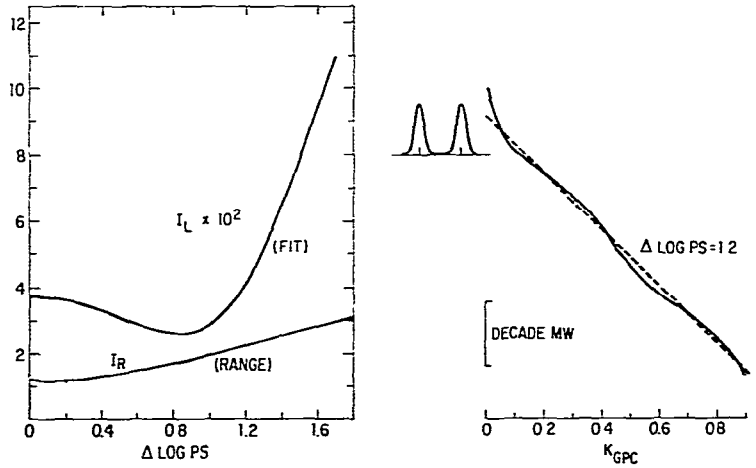

Fig. 8. Effect of pore size distribution on calibration linearity and molecular weight range: bimodal. Pore size distribution (PSD) = 0.15; pore volume ratio (VPR) = 1.0.

These results show that a pore volume mismatch favoring the macropores (large) over the mesopores (small) still produces a good linear fit. However, the opposite is not true. This conclusion is again reflected in the I_L at the left of Fig. 10. The reason for the desirability of having a slightly larger (up to *ca.* 20%) pore volume for the macropores is because the resolution of a single PS is distributed unevenly between the high and the low MW region of the calibration graph. In Fig. 10, the effect of pore volume mismatch on I_L and I_R is illustrated for both PSD = 0 and 0.15 with the curves showing the same general trend with only minor differences. Fig. 11 shows that a pore volume mismatch in favor of macropores also has only a minor effect on the MW error of broad MWD analyses.

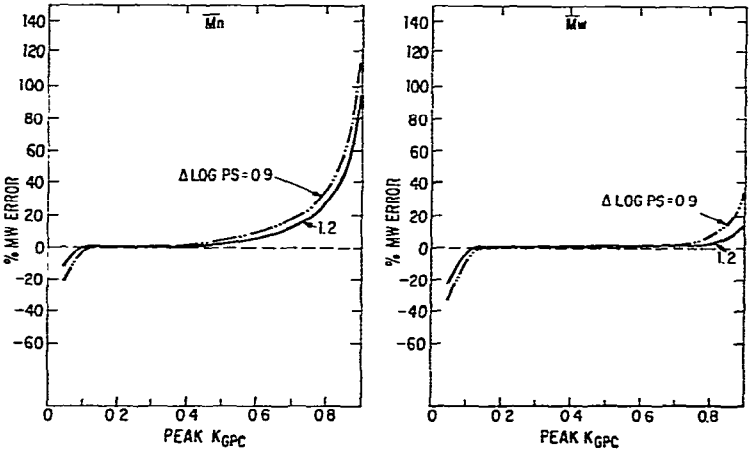

Fig. 9. Effect of polymer with Flory molecular weight distribution on molecular weight errors: bimodal. Conditions as in Fig. 8.

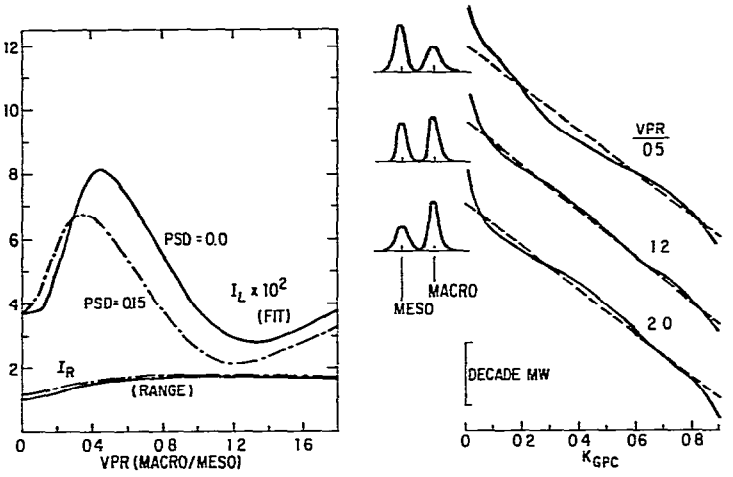

Fig. 10. Effect of pore volume ratio for bimodal system on calibration linearity and molecular weight range. Δlog PS = 0.9.

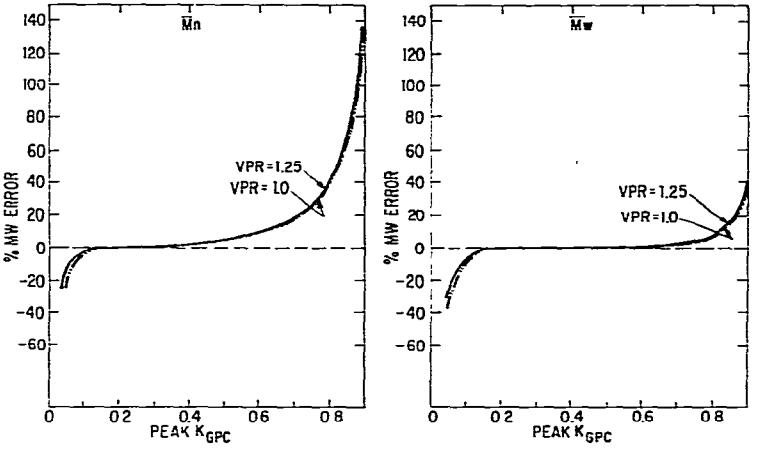

Fig. 11. Effect of polymer with Flory molecular weight distribution on molecular weight errors: bimodal. Pore size distribution (PSD) = 0.15; Δlog PS = 0.9.

Discussion

The calibration graphs and related MW errors from the simulation are presented in terms of polystyrene MW units in tetrahydrofuran solvent, so the concept of bimodal approach can be explained in the terminologies that are familiar to GPC users. However, this choice of a specific polymer–solvent system for presentation purposes does not affect the general conclusions of the study. It should be noted that the I_L and I_R curves are presented in terms of the more basic polymer size parameter, R_g. Therefore, these plots are applicable to different polymer–solvent systems in general. By using appropriate k and α values in eqn. 2, the I_L and I_R curves can be converted into MW error and separation ranges for any other polymer–solvent systems. As temperature, solvent and polymer type affect only the k and α values but

not the form of eqn. 2, the conclusions for optimizing column selections should be generally applicable. A linear column set optimized for polystyrene should perform equally well for other polymer and solvent systems in general.

Several specific theoretical models were used in this simulation study and the effects of other models were not fully explored. However, we believe that the present choices of pore shape and polymer MWD models are realistic. The choice of the log-normal PSD model is rather arbitrary. However, the actual PSD varies greatly and it is not possible to describe this function accurately by any one model. We expect that the conclusions of this study should be generally accurate, except possibly for PSD with very peculiar shapes.

A versatile, general-purpose bimodal GPC column set should have a linear MW range of about 4 decades, from a MW of a few hundreds to a few millions, to handle most commercial polymers adequately. It is generally best not to over-extend the MW range unnecessarily by increasing the Δlog PS of the pores. A wider MW range sacrifices resolution by changing the slope of the calibration graph, and increases the MW errors caused by finite column dispersion. As mentioned earlier, however, this sacrifice in resolution and increase of dispersion-caused MW errors is generally small in high-performance GPC because of the initial high resolution of such systems[3].

ARRANGEMENT OF BIMODAL COLUMN SETS

Experimental

Bimodal PSD packings simplify the SEC techniques by providing data suitable for MW calculations based on linear retention volume–log MW relationships[17]. Sets of commercial columns can be arranged to provide approximate bimodal PSD for separation, if the PS and internal pore volume of the separate columns combine to meet the criteria established in the sections above.

The additive nature of column internal pore volume is easily recognized. A series of connected SEC columns will provide a separation volume equal to the sum of the separation volumes of each separate column. As with all chromatographic techniques, the required internal volume of a column set is determined by the resolution requirements of the experiment. Increasing the column length increases the separation volume and thus increases resolution.

The separation capacities of separate columns are also additive. At a specific MW the separation capacity of a set of columns is the sum of the separation capacity of the individual columns of the set at that MW[19,20]. In the linear approximation, where $V_R = C_1 - (C_2 \log \mathrm{MW})$, C_2 represents the separation capacity of the column set. A wide-range linear calibration requires that C_2 values remain constant over 4–5 decades of MW. Therefore, the sum of the C_2 values for the individual columns must also remain constant over the same MW range. The calibration plot in Fig. 12 illustrates the traditional approach of connecting columns with different PS to obtain fractionation over a wide MW range. However, this approach produces relatively large deviations from a linear fit with a linearity range of less than 3 decades. In effect, this arrangement is analogous to using a single PS with a very broad PSD. The poor linear fit and limited linear range is not surprising in view of the results shown for the monomodal system in Fig. 3 (PSD = 0.65).

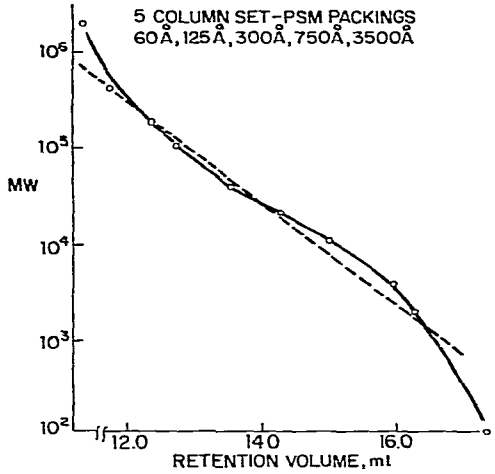

Fig. 12. Calibration plot from traditional approach of connecting columns of different pore sizes. Columns, 10 × 0.78 cm each, porous silica microspheres[8]; mobile phase, tetrahydrofuran, 22°; flow-rate, 2.5 ml/min; UV detector, 254 nm; sample, 25 μl of polystyrene standard solutions.

On the other hand, the bimodal size-exclusion concept discussed above indicates that the best way to achieve a constant sum of separation capacity is to allocate the required pore volume to PS that do not have significantly overlapping MW separation ranges. Thus, the separation capacity for a 2-decade MW range (*i.e.*, MW 10^3–10^5) is controlled by the properties of one PS column, while the adjacent, but not overlapping MW range (*i.e.*, MW 10^5–10^7) is controlled by the characteristics of a second PS column. Fig. 13 shows the relationship of pore size to the separation range

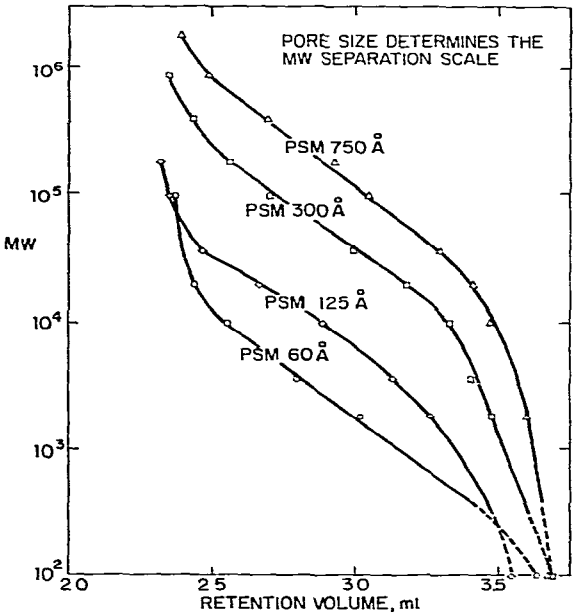

Fig. 13. Molecular weight calibration range as a function of pore size. Conditions as in Fig. 12.

of some narrow PSD silica columns. These GPC calibration graphs were determined by plotting the peak retention volumes of a series of narrow MWD polystyrene standards. Note that the slopes (separation capacity) of these calibration graphs are similar regardless of PS.

The bimodal GPC theory predicts that wide-range linear calibrations are possible for column sets with bimodal PS differing by about 1 decade or more. However, a detailed knowledge of PS or PSD (*e.g.*, for commercial columns) is not required to assemble a column set that demonstrates a calibration graph with reasonable MW range and linearity fit. Inspection of Fig. 14 shows that the 60-Å porous silica microsphere[8] column fractionates between *ca.* MW 10^2 and 10^4 while the 750-Å column separates from *ca.* MW 10^4 to 10^6. As the separation capacities (slopes of the calibration graphs) are nearly identical within these respective MW limits, a combination of these two columns gives the calibration graph shown in Fig. 15 with about 4 decades of linear MW range (200–10^6 MW shown at right) and an excellent fit. For this bimodal column set, $\Delta\log \text{PS} = \log PS_2/PS_1 = \log 750/60 = 1.10$, and from Fig. 8, this corresponds to $I_R = 2.15$. Converting from the radius of gyration range to linear molecular weight range for polystyrene (Table I) gives $I_{MW} = 3.7$. This represents 3.7 decades of linearity calculated from theory, closely corresponding to the 4 decades observed experimentally. This small difference supports the validity of the theoretical model used in the simulation study. MW errors for this column set can be predicted from Fig. 9.

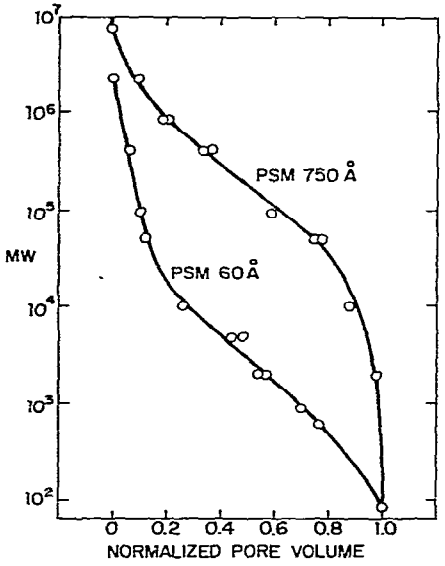

Fig. 14. Comparison of molecular weight fractionation range for particles with pore sizes differing by about 1 decade. Conditions as in Fig. 12.

Resolution of the linear column set can be increased by using additional columns of the same PS, but always in the same proportion to provide an equivalent pore volume for each PS. Even wider linear MW calibration ranges can be obtained with the bimodal approach, if desired. Fig. 16 shows the MW calibration for a set of

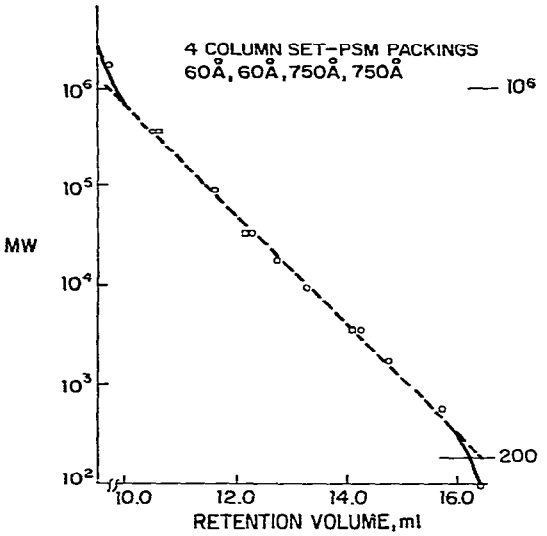

Fig. 15. Polystyrene molecular weight calibration graph with bimodal column set. Conditions as in Fig. 12.

47-Å and 1200-Å columns which exhibits almost 5 decades of MW linearity. It should be realized that at MW $< 10^3$ the random coil model for polymers becomes less definitive, but in this case the data for the standards still fall on a linear calibration plot. For this set, Δlog PS = 1.41 (Fig. 8), corresponding to $I_R = 2.6$, and a suggested linear range of 4.4 decades, compared with almost 5 decades, is shown in the experimental plot. Of course, the larger I_L value observed for this pore size difference ($I_L = 1.4$ compared with 1.1 for the 4-decade system in Fig. 15) is indicative of the larger MW errors that would result. However, as inferred by the data in Fig. 9, this increase in MW error is modest, and in many instances would be acceptable in view of the added versatility and convenience of the increased range of linear calibration.

Separation characteristics of 30-cm commercial μ-Styragel and 10-cm experimental porous silica microsphere columns[8] are summarized in Fig. 17. The separation capacity was determined by estimating the slope of a straight-line fit through the linear portion of the polystyrene peak position calibration graph for each column. The MW separation range was determined by limiting the calibration graph to a $\pm 20\%$ MW error window drawn parallel to the straight line. No correction has been made for differences in column length between the gel and silica columns.

Data such as those in Fig. 17 can be used to predict the shape of an SEC calibration graph. Suppose, for example, that a "500-Å" and a "10^5-Å" μ-Styragel column were connected. The MW separation range of the "500-Å" column does not overlap that of the "10^5-Å" column, but is sufficiently close to provide continuity in the separation of molecular weight species from *ca.* MW 500 to $2 \cdot 10^6$. However, the calibration graph would show a sharp change of slope near MW 20,000 because of the differences in separation capacities (C_2) of the two columns. To equalize the separation capacities, the pore volume associated with "500-Å" μ-Styragel must be increased about 2-fold. Thus, in this example, a linear μ-Styragel set could be obtained with two 30-cm "500-Å" μ-Styragel columns coupled to a single "10^5-Å" μ-

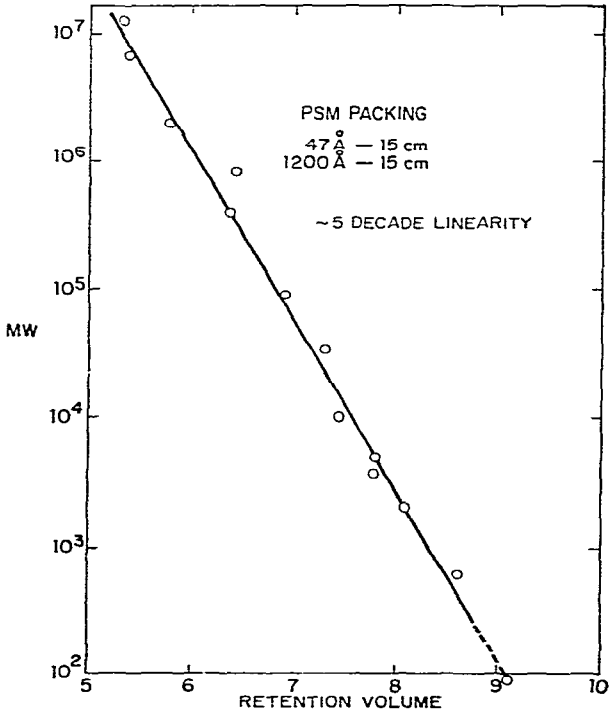

Fig. 16. Very wide linear molecular weight range calibration graph with bimodal column set. Conditions as in Fig. 12.

Styragel column. Approximately linear calibrations with the bimodal approach can often be easily obtained with commercial columns if the calibration plots are known or can be measured.

Unfortunately, the characteristics of gel packings appear to vary from lot to lot and from solvent to solvent. For example, the two "10^3-Å" μ-Styragel columns shown in Fig. 17 differ significantly in pore size (different MW separation ranges) and internal volume (different separation capacities, C_2). Direct substitution of one "10^3-Å" μ-Styragel column for another in a column set without prior information would lead to changes in the shape of the calibration graph of the set and alteration of the linear range and fit. Lot-to-lot variation could limit the versatility of gel packings for wide-range linear column set arrangement.

On the other hand, columns of the porous silica microspheres (PSM)[8] appear almost ideal for the bimodal approach. As illustrated by the data in Fig. 17, particles of various PS have virtually identical and reproducible separation capacities and range because of the consistent pore structure and specific porosity defined by the method of synthesis[4,5]. In addition, the PS ranges of the PSM permit readily constructed and optimized bimodal GPC systems. Further, the PSM have narrow PSD (generally <0.1) and small size (6–7 μm) to maintain separation resolution and good MW accuracy in GPC analyses[3]. The rigid PSM also have the usual mechanical advantages over semi-rigid gel microparticles. Finally, bimodal calibration graphs for

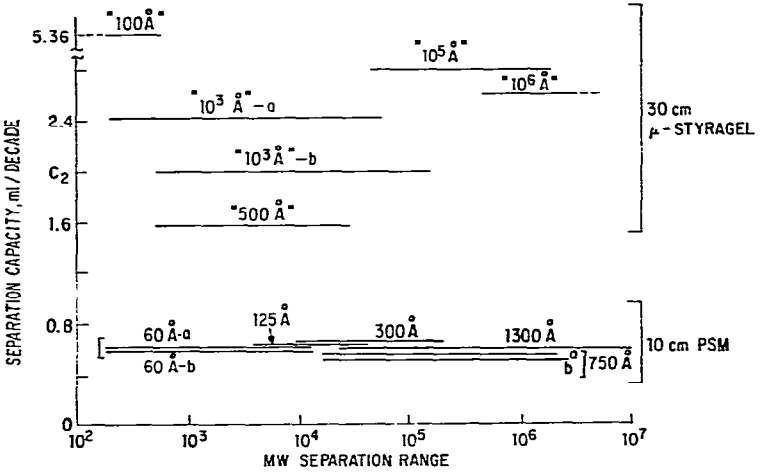

Fig. 17. Separation capacity *versus* calibration range for μ-Styragel and porous silica microsphere columns. Data on PSM columns obtained same as for Fig. 12. μ-Styragel data obtained using: mobile phase, tetrahydrofuran, 23°; flow-rate, 1.0 ml/min; detector, RI; sample, 100 μl of polystyrene standard solutions.

the PSM particles can be predicted from PSD data (*e.g.*, from mercury porosimetry,) which is not possible with semi-rigid organic gels.

Single particles with bimodal pore distribution

Bimodal pore distributions also can be obtained in single particles for optimized MW linearity range in SEC systems. Porous microspheres with two PS of the type shown schematically in Fig. 18 were synthesized by multilayering 2000-Å silica sol particles (procedure in ref. 21) on to porous silica microspheres, PSM-40 (50-Å mesopores, 351 m^2/g, 8.4-μm diameter[22]). The porous spherical inner core of the macroparticle consists of aggregated spherical 50-Å ultramicroparticles, and a 1.5–2-μm skin is composed of spherical 2000-Å microparticles. Mesopores are formed between the individual ultramicroparticles, and macropores between the microparticles. Mercury intrusion characterization of these 10-μm particles is shown in Fig. 19. This material shows mesopores with a mean diameter of 50 Å (specific porosity, 0.31 cm^3/g) and macropores at 650 Å (specific porosity, 0.20 cm^3/g). The ratio of the macropore to mesopore volumes, VP_2/VP_1, is 0.65, which is somewhat out of the optimal range for linear fit of calibration, but still near optimum for wide linear calibration range (see bottom curve, left, Fig. 10).

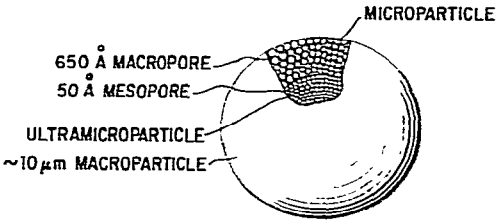

Fig. 18. Schematic diagram of bimodal porous particle.

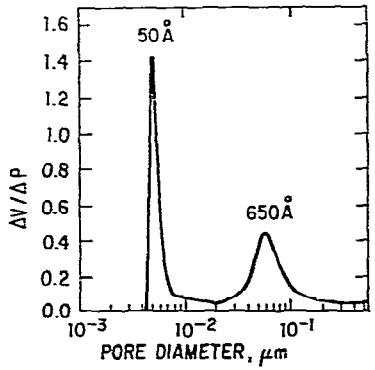

Fig. 19. Mercury porosimetry of bimodal particles.

The polystyrene MW *versus* retention volume, V_R, calibration for a column of these bimodal porous silica microbeads is shown in Fig. 20. The relationships in Fig. 8 for PSD = 0.15 (actual for bimodal particle, PSD = 0.09 and 0.13, for mesopores and macropores, respectively), predict a linear range, Δlog PS = 1.11, I_R = 2.15 and linear MW range for polystyrene of 3.7 decades. This value of 3.7

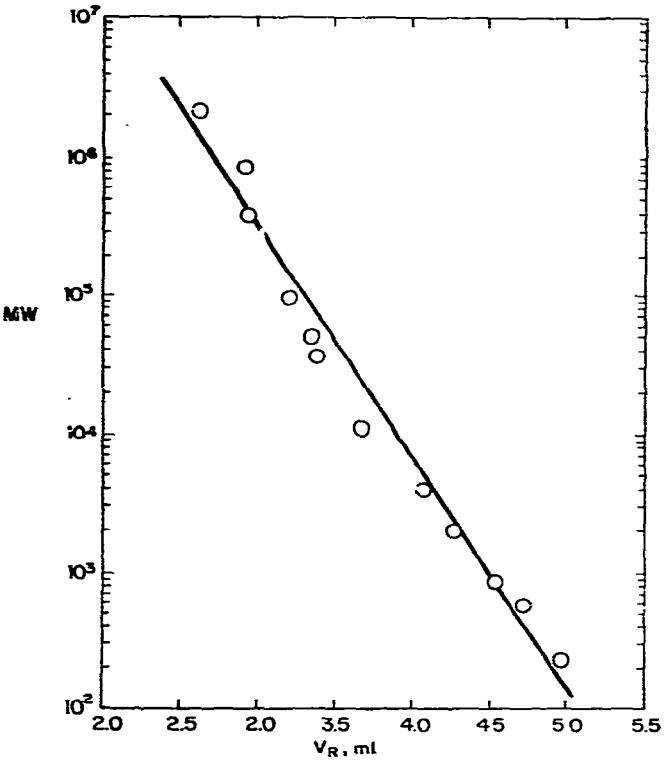

Fig. 20. Polystyrene calibration graph for column of bimodal particles. Column, 25 × 0.62 cm, 50 Å/650 Å pores; mobile phase, tetrahydrofuran, 23°; flow-rate, 1.0 ml/min; detector, UV, 254 nm; sample, 25 μl of polystyrene standard solutions.

decades compares closely with the approximately four decades of linearity found for the column of porous bimodal particles in Fig. 20. These experimental data appear again to confirm the validity of the theoretical concepts used to determine criteria in bimodal SEC systems.

Thus, columns of single particles based on bimodal PSD can fulfil the requirements for maintaining an extended linear MW calibration range, resulting in increased GPC MW accuracy and improved convenience and versatility.

Superficially porous or pellicular macroparticles with bimodal PSD also have been synthesized. As illustrated in Fig. 21, these macroparticles are made from Zipax* chromatographic support (*ca.* 30 μm), which consists of an impervious macropore on to which a crust of microparticles has been multilayered, the spaces between the microparticles forming the macropores of the bimodal particle. To each microparticle is multilayered a crust of ultramicroparticles. The spaces between these ultramicroparticles make up the mesopores forming the other mode of the bimodal distribution. Mercury porosimetry of this sample showed a break at about 0.07 μm (700 Å), representing the pores between the large sol particles in the crust of the initial Zipax structure, and a break at about 0.006 μm (60 Å), representing the pores between 140-Å sol particles that were multilayered on to the original Zipax structure. The specific porosities associated with the bimodal PSD were: 700-Å pores, 0.011 cm^3/g; 60-Å pores, 0.014 cm^3/g. Based on the mercury intrusion data, the bimodal pellicular particles exhibit $\Delta \log PS = 1.07$ and a macropore to mesopore volume ratio of $VP_2/VP_1 = 0.79$. No chromatographic tests have been carried out on these particles. However, it is anticipated that, while wide-linear calibrations should result, resolution of polymers with these particular particles would be relatively poor because of their low specific porosity. A better application of these particles could be for characterizing inorganic colloids by SEC because of the very favorable mass transfer characteristics. Such applications could be important for these particles, providing the specific porosity of the porous crust can be increased.

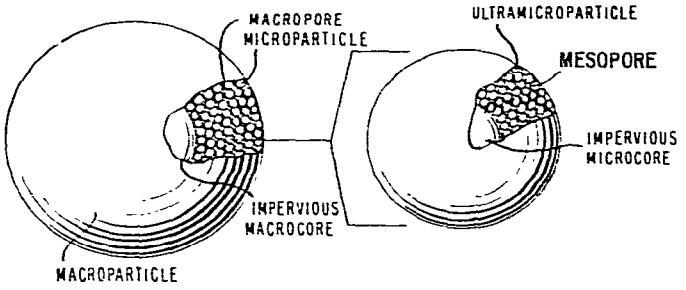

Fig. 21. Schematic diagram of pellicular particle with bimodal pore distribution.

CONCLUSIONS

A quantitative description of the effect of PSD on GPC separation has been developed. We now can predict the shape of GPC calibration graphs for various col-

* Zipax: DuPont registered trademark for a chromatographic support.

umn combinations. The performance of the column sets can be evaluated quantitatively in terms of the versatility (MW range) and MW accuracy (linearity fit) from their calibration graphs.

The results of these studies show the following.

(1) Use of bimodal PSD is the best approach to achieve a versatile, general-purpose column set for broad GPC MW separation range (up to 5 decades of MW).

(2) The bimodal configuration is always superior in MW range and MW accuracy to monomodal systems and column sets with several overlapping MW ranges.

(3) A bimodal column set designed for optimal performance using one polymer–solvent system should function equally well in other systems.

(4) The recommended bimodal PSD approach is to maintain about 1 decade difference in average PS and approximately equal pore volumes for the two PS.

(5) If there is moderate PSD of the two groups of pores, a larger than 1 decade PS difference is required in order to achieve optimal bimodal column combination.

(6) Porous silica microsphere (PSM) packings are better suited for the bimodal approach than organic gel-type packings because:

(i) PS and PSD can be measured experimentally for PSM packings to facilitate bimodal organization;

(ii) PSM packings of different PS have consistent pore volume and PSD for convenient bimodal optimization;

(iii) optimal bimodal characteristics occur with rigid particles.

(7) For broad MWD polymer analyses, the MW errors expected from approximate linear calibration is larger for $\bar{M}_n$ than for $\bar{M}_w$.

(8) For Flory-type MWD polymers, the MW errors are the smallest when the polymer peak elutes at small distribution coefficient (K_{GPC}) regions (but not less than $K_{GPC} = 0.1$).

ACKNOWLEDGMENTS

We thank H. J. Stoklosa for his help with some of the calculations and C. H. Dilks, Jr., for his assistance with some of the experimental work.

GLOSSARY OF SYMBOLS

K_{GPC}	GPC distribution coefficient
β_m	mth root of the Bessel function of the first kind of order zero
R_g	Radius of gyration, or more accurately, the root-mean-square radius of gyration
a	Pore radius
M; MW	Molecular weight
k and α	Amplitude and exponent constant of the R_g *vs.* M relationship (eqn. 2).
PS	Pore size
PSD	Standard deviation in log PS units of a log-normal PSD curve
I_R	Index of separation range expressed in units of log R_g
I_{MW}	MW separation range in units of log MW

I_L	Index of linearity in units of log R_g
n	Number of data points used to calculate the linearity fit
VP and VPR	Pore volume and pore volume ratio of the macropore over the mesopore in a bimodal PSD
ε_{MW}	Average MW error (%) over the separation range resulting from deviations from linear calibration graph
W_M	Weight fraction of a polymer MWD
M_0	MW of the repeating unit in a polymer
p	Extent of a polymerization reaction
$\bar{M}_w$ and $\bar{M}_n$	Weight- and number-average molecular weight, respectively
VP_2 and VP_1	Macropore and mesopore volume, respectively.

REFERENCES

1 Waters Associates, Technical Bulletin, *Know More About Your Polymers*, AN 155, Waters Assoc., Milford, Mass., 1975.
2 M. R. Ambler, L. J. Fetters and Y. Kesten, *J. Appl. Polym. Sci.*, 21 (1977) 2439.
3 W. W. Yau, J. J. Kirkland, D. D. Bly and H. J. Stoklosa, *J. Chromatogr.*, 125 (1975) 219.
4 J. J. Kirkland, in S. G. Perry (Editor), *Gas Chromatography 1972*, Applied Science Publ., Barking, 1973, p. 39.
5 L. R. Snyder and J. J. Kirkland, *Introduction to Modern Liquid Chromatography*, Wiley-Interscience, New York, 1974, Ch. 6.
6 J. J. Kirkland, *U.S. Pat.*, 3,782,075, 1974.
7 R. K. Iler and H. J. McQueston, *U.S. Pat.*, 3,855,172, 1974.
8 J. J. Kirkland, *J. Chromatogr.*, 125 (1976) 231.
9 J. J. Kirkland, *Chromatographia*, 8 (1975) 661.
10 J. S. Fok and E. A. Abrahamson, *Chromatographia*, 7 (1974) 423.
11 J. S. Fok and E. A. Abrahamson, *Amer. Lab.*, 7 (1975) 63.
12 A. T. James and A. J. P. Martin, *Analyst (London)*, 77 (1952) 915.
13 E. F. Casassa and Y. Tagami, *Macromolecules*, 2 (1969) 14.
14 W. W. Yau, *J. Polym. Sci., Part A-2*, 7 (1969) 483.
15 H. Coll and D. K. Gilding, *J. Polym. Sci., Part A-2*, 8 (1970) 89.
16 J. M. Evans and L. J. Maisey, in J. H. S. Green and R. Dietz (Editors), *Industrial Polymers: Characterization by MW*, Transcripta Books, London, 1973.
17 W. W. Yau, H. J. Stoklosa and D. D. Bly, *J. Appl. Polym. Sci.*, 21 (1977) 1911.
18 P. J. Flory, *Principles of Polymer Chemistry*, Cornell Univ. Press, Ithaca, N.Y., 1953.
19 Y. Ishida, S. Ueda, K. Kawai and I. Kimura, *Kobunski Kagaku (Chem. High Polym.)*, 27 (1970) 33.
20 T. E. Saunders and T. K. Rehfeldt, *J. Chromatogr. Sci.*, 11 (1973) 511.
21 J. J. Kirkland, *U.S. Pat.*, 3,505,785, 1970.
22 J. J. Kirkland and P. E. Antle, *J. Chromatogr. Sci.*, 15 (1977) 137.